

Effects of TMIn flow rate during quantum barrier growth on multi-quantum well material properties and device performance of GaN-based laser diodes

Zhenyu Chen(陈振宇), Degang Zhao(赵德刚), Feng Liang(梁锋), Zongshun Liu(刘宗顺), Jing Yang(杨静), and Ping Chen(陈平)

Citation: Chin. Phys. B, 2024, 33 (**12**): 128102. DOI: 10.1088/1674-1056/ad8624
Journal homepage: http://cpb.iphy.ac.cn; http://iopscience.iop.org/cpb

What follows is a list of articles you may be interested in

Butt-joint regrowth method by MOCVD for integration of evanescent wave coupled photodetector and multi-quantum well semiconductor optical amplifier

Feng Xiao(肖峰), Qin Han(韩勤), Han Ye(叶焓), Shuai Wang(王帅), Zi-Qing Lu(陆子晴), and Fan Xiao(肖帆)
Chin. Phys. B, 2022, 31 (**4**): 048101. DOI: 10.1088/1674-1056/ac272b

Characterization of the N-polar GaN film grown on C-plane sapphire and misoriented C-plane sapphire substrates by MOCVD

Xiaotao Hu(胡小涛), Yimeng Song(宋祎萌), Zhaole Su(苏兆乐), Haiqiang Jia(贾海强), Wenxin Wang(王文新), Yang Jiang(江洋), Yangfeng Li(李阳锋), and Hong Chen(陈弘)
Chin. Phys. B, 2022, 31 (**3**): 038103. DOI: 10.1088/1674-1056/ac3bad

Effect of nitrogen gas flow and growth temperature on extension of GaN layer on Si

Jian-Kai Xu(徐健凯), Li-Juan Jiang(姜丽娟), Qian Wang(王茜), Quan Wang(王权), Hong-Ling Xiao(肖红领), Chun Feng(冯春), Wei Li(李巍), and Xiao-Liang Wang(王晓亮)
Chin. Phys. B, 2021, 30 (**11**): 118101. DOI: 10.1088/1674-1056/abff30

Continuous-wave operation of InAs/InP quantum dot tunable external-cavity laser grown by metal-organic chemical vapor deposition

Yan Wang(王岩), Shuai Luo(罗帅), Haiming Ji(季海铭), Di Qu(曲迪), and Yidong Huang(黄翊东)
Chin. Phys. B, 2021, 30 (**1**): 018106. DOI: 10.1088/1674-1056/abcfa4

Suppression of electron and hole overflow in GaN-based near-ultraviolet laser diodes

Yao Xing(邢瑶), De-Gang Zhao(赵德刚), De-Sheng Jiang(江德生), Xiang Li(李翔), Zong-Shun Liu(刘宗顺), Jian-Jun Zhu(朱建军), Ping Chen(陈平), Jing Yang(杨静), Wei Liu(刘炜), Feng Liang(梁锋), Shuang-Tao Liu(刘双韬), Li-Qun Zhang(张立群), Wen-Jie Wang(王文杰), Mo Li(李沫), Yuan-Tao Zhang(张源涛), Guo-Tong Du(杜国同)
Chin. Phys. B, 2018, 27 (**2**): 028101. DOI: 10.1088/1674-1056/27/2/028101

Effects of TMIn flow rate during quantum barrier growth on multi-quantum well material properties and device performance of GaN-based laser diodes

Zhenyu Chen(陈振宇)[1,2], Degang Zhao(赵德刚)[1,3,†], Feng Liang(梁锋)[1,‡], Zongshun Liu(刘宗顺)[1], Jing Yang(杨静)[1], and Ping Chen(陈平)[1]

[1] *State Key Laboratory of Integrated Optoelectronics, Institute of Semiconductors, Chinese Academy of Sciences, Beijing* 100083, *China*
[2] *College of Materials Science and Opto-Electronic Technology, University of Chinese Academy of Sciences, Beijing* 100049, *China*
[3] *Center of Materials Science and Optoelectronics Engineering, University of Chinese Academy of Sciences, Beijing* 100049, *China*

(Received 23 August 2024; revised manuscript received 30 September 2024; accepted manuscript online 12 October 2024)

Multidimensional influences of indium composition in barrier layers on GaN-based blue laser diodes (LDs) are discussed from both material quality and device physics perspectives. LDs with higher indium content in the barriers demonstrate a notably lower threshold current and shorter lasing wavelength compared to those with lower indium content. Our experiments reveal that higher indium content in the barrier layers can partially reduce indium composition in the quantum wells, a novel discovery. Employing higher indium content barrier layers leads to improved luminescence properties of the MQW region. Detailed analysis reveals that this improvement can be attributed to better homogeneity in the indium composition of the well layers along the epitaxy direction. InGaN barrier layers suppress the lattice mismatch between barrier and well layers, thus mitigating the indium content pulling effect in the well layers. In supplement to experimental analysis, theoretical computations are performed, showing that InGaN barrier structures can effectively enhance carrier recombination efficiency and optical confinement of LD structure, thus improving the output efficiency of GaN-based blue LDs. Combining these theoretical insights with our experimental data, we propose that higher indium content barriers effectively enhance carrier recombination efficiency and indium content homogeneity in quantum well layers, thereby improving the output performance of GaN-based blue LDs.

Keywords: laser diodes, MOCVD, quantum wells, III–V semiconductors

PACS: 81.15.Gh, 78.67.De, 42.55.Px, 81.05.Ea **DOI:** 10.1088/1674-1056/ad8624

1. Introduction

GaN-based laser diodes (LDs) have garnered significant interest owing to their tunable wavelength, with numerous reports on their advancements in recent years.[1,2] Various research groups have successfully developed high-performance ultraviolet, violet, blue, and green LDs,[2–5] reflecting the versatility and potential applications of GaN-based LDs. Particularly, blue light, as one of the primary colors, finds utility in laser displays, underwater communications,[6] and high-power laser processing, underscoring the broad research prospects for high-power GaN-based blue lasers.[7] In the pursuit of enhancing the efficiency of blue LDs, the design of the multi-quantum well (MQW) structure holds paramount importance. Typically, the well layer of the quantum well employs InGaN material with higher indium composition, while the quantum barrier layer has various choices, including GaN, InGaN, and AlInGaN structures for stress compensation.[8,9] Several studies have proposed structural designs for GaN MQWs, encompassing LED and LD structures.

Considerations for barrier layer design primarily stem from three directions. Firstly, stress compensation is a crucial aspect. Park *et al.*[10–12] demonstrated that employing InGaN barrier layers in blue and green LEDs effectively mitigates lattice mismatch, thereby augmenting the radiative recombination rate of MQW. This leads to LEDs with higher internal quantum efficiency and improved output light intensity. Fu *et al.*[13] employed an AlInGaN barrier layer to enable independent adjustment of components and lattice constants, thereby optimizing lattice mismatch and enhancing radiative recombination efficiency. Secondly, carrier injection efficiency is another critical consideration. Various researchers, including Kuo *et al.*,[14] Wang *et al.*[15] and Wang *et al.*,[16] have utilized component-graded barrier layer structures in LEDs through simulation, effectively improving injection efficiency and mitigating droop effects. Yang *et al.*[17] employed a structure alternately utilizing InGaN and GaN barrier layers to reduce leakage current, enhance carrier recombination efficiency, and improve internal quantum efficiency. Furthermore, Noh *et al.*[18] utilized superlattice barrier layers with varying indium compositions to improve IQE in LEDs. However, due to differences in structure and design objectives, several effective methods[18–20] for improving LED performance are not applicable to LDs. In LD structures, apart from stress compensation and carrier injection efficiency, nonradiative recombina-

†Corresponding author. E-mail: dgzhao@semi.ac.cn
‡Corresponding author. E-mail: liangfeng13@semi.ac.cn

© 2024 Chinese Physical Society and IOP Publishing Ltd

tion center density and the distribution of the light field also warrant attention. A concentrated light field in the active area enhances laser performance. Cheng *et al.*[8] conducted simulations to investigate the impact of laser barrier layer selection on light field leakage. Ben *et al.*[21] demonstrated through simulation calculations that selecting InGaN for the barrier layer can optimize light field leakage to a certain extent. More importantly, opting for InGaN barrier layers can enhance quantum well uniformity, thereby improving the mode gain.

The prevailing research in LDs primarily compares the performance disparities attributed to GaN barrier layers versus InGaN or AlInGaN barrier layers, generally concluding that InGaN barrier layers exhibit superior performance. However, there is still a lack of detailed investigation concerning different indium compositions in InGaN barriers. In our study, we addressed this gap by refining this aspect computationally through LASTIP simulation. Moreover, compared to LED structures, LDs impose higher demands on the quality of quantum wells, rendering the factors influencing the selection of quantum barriers more intricate. Much of the current research, particularly concerning LD structures, relies heavily on simulations. However, it is well understood that for GaN materials, owing to challenges in material growth, there often exist disparities between simulation-derived conclusions and actual results. Divergent structures obtained through simulation calculations can lead to variations in quantum well materials during the metal–organic chemical vapor deposition (MOCVD) growth process, thereby impacting LD performance in distinct ways. Hence, in our study, we directed our focus towards analyzing the differences in quantum well quality arising from diverse barrier layer indium compositions, in supplement to simulation results. We also extended this analysis to encompass actual LD performance, thereby offering a more comprehensive understanding of the relationship between barrier layer material choice and LD performance.

2. Experiments

In this study, we employed both simulation methods and experimental techniques. During epitaxy, two LD samples, LD1 and LD2, and three MQW samples, labeled as samples A, B, and C were prepared. The epitaxial growth of both MQW samples and LDs utilized the Thomas-Swan close-coupled showerhead MOCVD equipment. The three MQW samples and two LD samples were all grown on 2-inch *c*-plane (0001) free-standing GaN substrates. Metal precursors were trimethylindium (TMIn), trimethylgallium (TMGa), trimethylaluminum (TMAl), bis-cyclopentadienyl magnesium (Cp_2Mg), silane (SiH_4), and ammonia (NH_3) for In, Ga, Al, Mg, Si, and N, respectively. Hydrogen (H_2) was utilized as the carrier gas during the growth of the quantum well structure, including both quantum wells and quantum barriers. Nitrogen (N_2) served as the carrier gas for all other layers.

A schematic diagram of the LD structure for both samples LD1 and LD2 is depicted in Fig. 1(a). It comprises a 150 μm thick n-GaN substrate (Si doping $= 3\times10^{18}$ cm^{-3}), followed by a 600 nm thick n-$Al_{0.08}Ga_{0.92}N$ lower cladding layer (LCL) (Si doping $= 3\times10^{18}$ cm^{-3}), a 200 nm thick n-$In_{0.04}Ga_{0.96}N$ lower waveguide layer (LWG) (Si doping $= 1\times10^{17}$ cm^{-3}), followed by a two-period InGaN multi-quantum well (MQW) active region designed for a target lasing wavelength of 440 nm. The MQW active region consists of two 3.5 nm thick $In_{0.12}Ga_{0.88}N$ quantum well layers sandwiched by three 10 nm thick $In_xGa_{1-x}N$ quantum barrier layers. Following the MQW region is a 200 nm thick n-$In_{0.04}Ga_{0.96}N$ upper waveguide layer (UWG) (Si doping $= 1\times10^{17}$ cm^{-3}), a 20 nm thick p-$Al_{0.15}Ga_{0.85}N$ electron blocking layer (EBL) (Mg doping $= 1\times10^{19}$ cm^{-3}), a 600 nm thick p-$Al_{0.08}Ga_{0.92}N$ upper cladding layer (UCL) (Mg doping $= 2\times10^{19}$ cm^{-3}), and a 40 nm thick p-GaN contact layer (Mg doping $= 1\times10^{20}$ cm^{-3}). The epitaxial structure underwent annealing in nitrogen gas at 900 °C for 180 s in order to activate Mg acceptors. Post epitaxial growth, the ridge waveguide structure was created. Initially, a 30-μm-wide ridge stripe was fabricated through photolithography and etching along the $(1\bar{1}00)$ direction. Subsequently, a 1200-μm-long cavity was formed by cleaving along the $\{1\bar{1}00\}$ plane after grounding and polishing the GaN substrate. Ti/Pt/Au and Pd/Pt/Au were utilized for n-type and p-type electrode contacts, respectively. The growth conditions for the two LD samples, LD1 and LD2, were identical except for the TMIn flow rate during the InGaN barrier growth, 20 sccm for LD1 and 15 sccm for LD2.

As illustrated in Fig. 1(b), the epitaxial structure of the MQW samples comprised a 23 nm GaN nucleation layer, a 1.5 μm unintentionally doped GaN layer, a 1 μm Si-doped n-GaN layer (Si doping $= 3\times10^{18}$ cm^{-3}), a 200 nm thick n-$In_{0.04}Ga_{0.96}N$ layer (Si doping $= 3\times10^{18}$ cm^{-3}) in order to simulate the strain environment of LD structure, a two-period InGaN MQW active region identical to that of the LD samples, a 150 nm thick p-GaN layer (Mg doping $= 2\times10^{19}$ cm^{-3}) and a 40 nm thick p-GaN contact layer (Mg doping $= 1\times10^{20}$ cm^{-3}). The epitaxial structure underwent annealing in nitrogen gas at 900 °C for 180 s in order to activate Mg acceptors. The growth conditions for the three MQW samples — A, B, and C — were identical and employing exactly the same method as MQW in LD samples, except for the TMIn flow rate during the InGaN barrier growth, which was set as 0 sccm for sample A, 15 sccm for sample B, and 20 sccm for sample C.

LASTIP was utilized during simulation, with specific structure parameters derived entirely from the experimental LD samples shown in Fig. 1(a), except for the indium content in the quantum well layers. The indium content in the

quantum well layers was set to 18% to achieve the target lasing wavelength of 440 nm during simulation. Five different sets of samples were established with identical structure parameters, except for the indium composition in the quantum barriers, varying from 0% to 4%. The energy band parameters and effective refractive index data were obtained from works from Laws *et al.* and Mhala *et al.*[22,23]

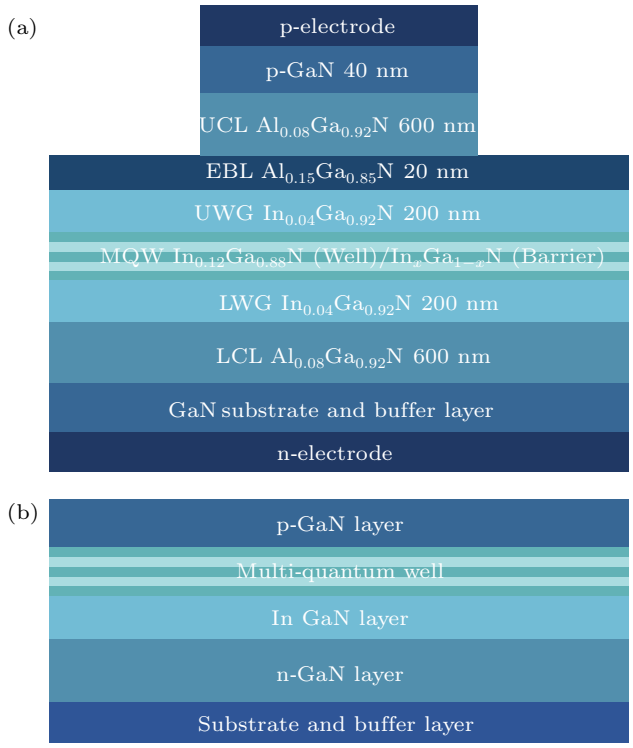


Fig. 1. Schematic diagram of LD samples (a) and MQW samples (b).

The MQW samples were characterized using various tools. Room temperature electroluminescence (EL) spectra were recorded using an Ocean Optics HR200 high-resolution spectrometer operating in direct current (DC) mode. Temperature-dependent photoluminescence (TDPL) spectra were obtained using a He–Cd laser (lasing wavelength: 325 nm). Microscopic photoluminescence (micro-PL) measurements with high spatial resolution were conducted using a Nikon A1 confocal optical system, with excitation provided by a 405 nm semiconductor laser. The structural properties of the samples were analyzed using a Rigaku SmartLab high-resolution x-ray diffractometer (HRXRD). For a detailed examination of the MQW structure, cross-sectional images were acquired using a JEOL JEM-F200 scanning transmission electron microscopy (STEM). The LD samples underwent threshold current and lasing spectrum measurements using a silicon-based photodetector and a Keithley 2400 source meter, operating in pulse current mode. The pulse width was set at 500 ns, with a duty cycle of 0.05%. These comprehensive characterization techniques enabled a thorough assessment of the LD and MQW samples' performance and structural properties.

3. Results and discussion

3.1. LD performance with different indium compositions in barrier layers

The utilization of InGaN barriers instead of GaN barriers has been demonstrated to be effective for GaN-based LDs and LEDs, as corroborated by studies.[8,21] Nonetheless, there remains a paucity of research regarding the specific selection of indium composition in InGaN barriers in LDs. Building upon this consensus, we fabricated two distinct blue laser diodes on free-standing GaN substrates, employing varying TMIn flow rates during the barrier growth process.

In Fig. 2(a), the distribution of threshold currents of LD1 and LD2 is illustrated. Sixteen chips were extracted from each wafer to mitigate individual errors stemming from epitaxy and fabrication inhomogeneity. Chips from LD1, featuring higher barrier indium content, exhibit notably lower threshold currents. The average threshold current of chips is 846 mA for LD1 and 959 mA for LD2. Subsequently, we selected one representative LD chip from each wafer to ascertain the lasing wavelength. The lasing spectrum, presented in Fig. 2(b), was obtained under pulse work mode with a pulse width of 500 ns and a duty cycle of 0.05%. The lasing wavelength of LD1 is 444.5 nm, which is 3 nm shorter than LD2's 447.6 nm.

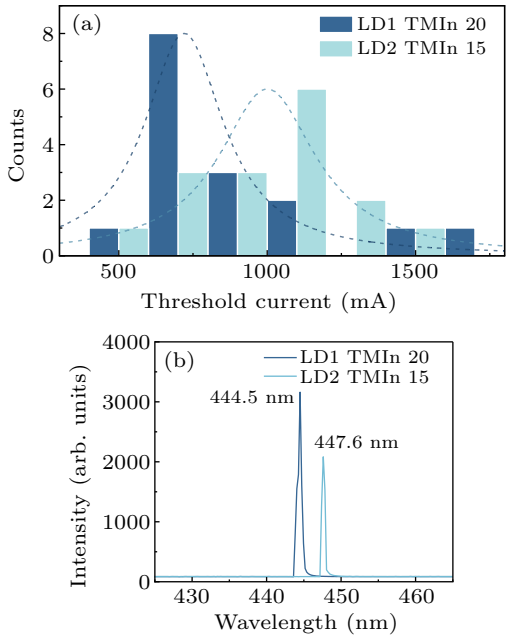


Fig. 2. (a) Histogram of threshold currents for LD1 and LD2, (b) lasing spectra of LD1 and LD2.

3.2. Influences on multi-quantum well structural and luminescence properties

As the structures are totally the same for these LDs except for the barrier indium content, the performance differences between LD1 and LD2 can be attributed to varieties in MQW structure and material quality. Thus, we prepared three MQW samples to characterize the MQW quality when

growing different indium composition barrier layers. Since we found that improving indium content in barrier layers will bring output efficiency improvement and lasing wavelength blue-shift, we need to find the roots of these two phenomena separately. Blue-shift of lasing wavelength is discussed first. During HRXRD measurement the $\omega/2\theta$ curves were obtained, and structure parameters of samples A, B, and C were determined through a numerical fitting to satellite peaks of these curves, as listed in Table 1. Considering possible fitting errors, the change in TMIn flow rate during barrier growth did not obviously affect the barrier thickness or well thickness. However, with an increase in TMIn flow rate from 0 sccm, 15 sccm to 20 sccm, the barrier indium content increased from 0% to 1.0% and then to 2.1%. It is noteworthy that this increasing process is not linear, which mainly results from surface reaction thermodynamics as reported by Lu *et al.*;[24] particularly, when the TMIn flow rate increased from 15 sccm to 20 sccm, the change in indium content was rather obvious. Additionally, as the TMIn flow rate increased, there appeared to be a decrease in the well indium content. We speculated that fitting errors may also affect this result. Therefore, we conducted electroluminescence tests to measure the emission wavelength of the samples, hoping that the emission wavelength at high injection currents could provide information of the exact indium content in the wells.

Table 1. Structure parameters of samples A, B, C obtained from fitting of HRXRD $\omega/2\theta$ curves.

Sample	A	B	C
TMIn (sccm)	0	15	20
Barrier indium (%)	0	1.0	2.1
Barrier thickness (nm)	10.6	10.6	10.6
Well indium (%)	11.4	11.0	10.6
Well thickness (nm)	3.7	3.7	3.7

We observed that the emission peak wavelengths of all three samples are stable when the injection currents increase from 50 mA to 100 mA during EL measurement as shown in Table 2. The FWHMs of EL peaks show a decreasing trend when increasing the TMIn flow rate as shown in Table 2, which indicates better luminescence homogeneity of samples with InGaN barriers. The emission wavelength exhibits a blue-shift as the injection current increases. This phenomenon occurs because the current injection shields the polarization field due to high carrier density.[25,26] In this scenario, the polarization field in the samples can be neglected at 100 mA. In such a condition the emission peak wavelength, as depicted in Fig. 3, can almost exactly reflect the energy gap of the InGaN wells. It is found that a blue-shift of the peak wavelength is evident in Fig. 3 as the TMIn flow rate increases. Such blue-shift aligns well with the LD lasing wavelengths results in Fig. 2(b).

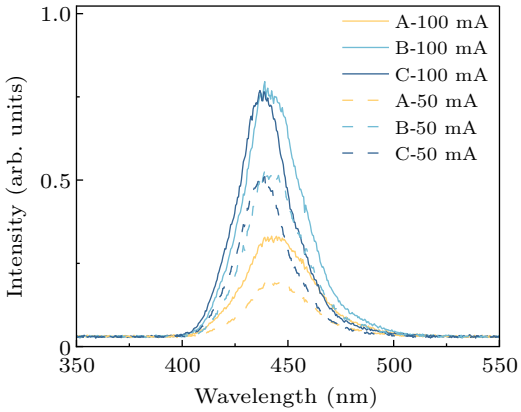


Fig. 3. Electroluminescence spectra of samples A, B and C at 50 mA and 100 mA injection current.

Table 2. EL peak wavelengths at 50 mA and 100 mA injection current of samples A, B and C.

Sample	A	B	C
TMIn (sccm)	0	15	20
Peak wavelength @50 mA (nm)	445.8	443.3	438.5
Peak wavelength @100 mA (nm)	445.7	442.9	438.7
FWHM @100 mA (nm)	30.2	27.7	24.9

We applied the HRXRD fitting results of the well indium content to the standard formula for the composition dependence of the bandgap of $In_xGa_{1-x}N$ at room temperature[22,27]

$$E_g = 3.4(1-x)+0.7x-3x(1-x).$$

Here, the bowing factor was obtained from McCluskey *et al.*[28] as 3 when referring to the approximate indium content in our samples as around 10%. This parameter was also recommended by Vurguftman *et al.*,[27] which is accurate when calculating the bandgap of relatively low indium content InGaN with practical LED or LD application. As shown in Table 3, the calculated emission wavelength based on the HRXRD fitting results corresponds well with the EL measurement results, confirming the reliability of the HRXRD fitting results. Thus, an intriguing finding emerges from this data set: higher TMIn flow rates during barrier growth can partly reduce the indium content in the wells.

Table 3. Calculated emission wavelength and EL peak wavelength of samples A, B and C.

Sample	A	B	C
TMIn (sccm)	0	15	20
Calculated well indium (%)	11.4	11.0	10.6
Calculated emission wavelength (nm)	445.7	442.9	438.7
EL peak wavelength @100 mA (nm)	446	443	439

This intriguing phenomenon requires further analysis, and we propose a possible hypothesis. Indium atom diffusion plays a significant role during heat treatment, particularly during the high-temperature growth of the p-type layer and thermal annealing following epitaxy. This heat treatment may lead

to the breaking of In–N bonds and facilitate indium atom diffusion near the interfaces between the barrier and well layers. As a result, a gradually varying indium content in the well layers develops along the epitaxial orientation. In samples B and C, the higher indium atom density increases the likelihood of In–In bond formation, which can induce the desorption of InGaN in the well layers. Consequently, the total indium content in the well layers shows a slight declining trend as the indium content in the barrier layers increases.

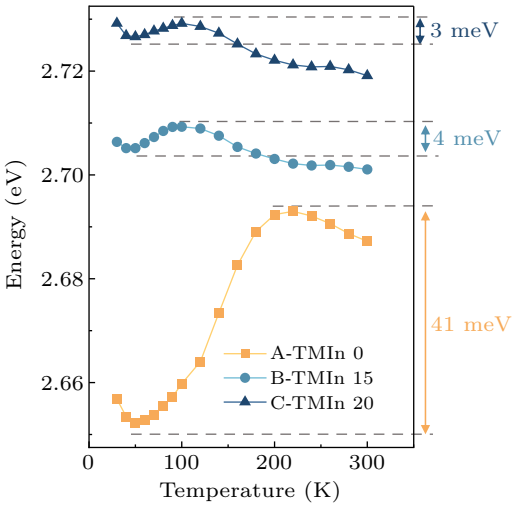


Fig. 4. Photoluminescence peak wavelengths at different testing temperatures for samples A, B and C.

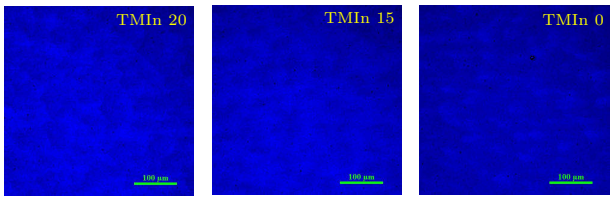


Fig. 5. Micro-PL images of samples A, B and C.

Apart from the indium content change in the well layers, further material quality characterization is warranted for these MQW samples, in order to explain the output efficiency differences in LD samples. Temperature-dependent photoluminescence (TDPL) was applied to further examine the luminescence properties of the MQW. The PL peak energies versus different testing temperatures from samples A, B, and C are shown in Fig. 4. Firstly, the PL energy exhibits an obvious blue-shift as the barrier TMIn flow rate increases, indicating a decrease in indium content in the quantum well, which corresponds well with XRD results. Furthermore, all three samples exhibit clear S-shaped peak shift curves in their TDPL results. However, the TDPL characteristics of sample A demonstrate significant differences compared to samples B and C. Regarding the S-shaped curves of the PL peak of InGaN materials, it has been reported in numerous literatures.[29–31] The redshift process at low temperatures is considered to be the result of charge carriers being activated by heat and filling to lower energy levels, while the redshift process at high temperatures is primarily dominated by the band gap shrinking process as the temperature increases.[30,32] The reasons for the blue-shift process are well-known as two kinds. One explanation is that the blue shift is related to local states, and the greater the blue shift in TDPL, the more uneven the distribution of local states in the InGaN layer, with a larger number of deep local states.[31] Another explanation is that the blue shift process is related to the competitive process of radiative recombination and non-radiative recombination, and the increase in the number of non-radiative recombination centers will result in stronger blue shift process of the sample.[33] In fact, both processes suggest that the greater the degree of blue shift during the TDPL peak position shift, the poorer the material quality or the homogeneity of the sample. In our samples, samples B and C exhibit a peak shift of 3–5 meV, while sample A demonstrates a remarkably higher blue-shift of 41 meV. To check the hypothesis relating to non-radiative recombination centers, we conducted micro-PL luminescence measurements on all three samples, as shown in Fig. 5.

Dark spots in micro-PL images typically indicate nonradiative recombination centers. However, in all three samples, no distinct differences can be observed, and all three samples exhibit uniform luminescence with small dark spots. From this, we can postulate that the difference in non-radiative recombination centers is not sufficient to account for the significant difference in TDPL peak shift observed among these samples. Furthermore, we have some reservations about explaining this phenomenon solely through local states. Typically, in InGaN quantum well materials, localized states stem from the uneven spatial distribution of the indium component in the quantum well, leading to a certain degree of fluctuation in the indium distribution.[34] Previous reports suggest that the presence of non-radiative recombination centers in micro-PL is closely related to the aggregation of indium components.[35] Since there is no significant difference observed in micro-PL, it is inferred that the degree of aggregation of indium components in the quantum wells is not significantly different among the samples.

Another important factor influencing the TDPL curve behavior is the shape of quantum wells. In the model that explains the origin of blue shift of the TDPL peak position by localized states, it essentially describes the carrier filling effect among different potential wells. If the energy level filling effect of the sample is stronger, the blue shift of the TDPL peak position will be greater. After removing the low-temperature red-shifted part, we applied the band tail filling model to fit the TDPL peak energy shift when the testing temperature is higher than 60 K:[36,37]

$$E_0(T) = E_0(0) - \frac{\alpha T^2}{T+\beta} - \frac{\sigma^2}{k_B T}.$$

Here, α and β are the Varshini fitting parameters, k_B is the Boltzmann's constant, and σ represents the degree of the energy level filling effect. The fitting results for σ are shown in Table 4.

Table 4. Fitting results of σ from samples A, B and C.

Sample	A	B	C
σ	34.18	8.63	8.35

It is evident that the energy level filling effect of samples B and C, with InGaN barrier layers, is significantly weaker compared to that of sample A, which utilizes GaN as the barrier layer. This discrepancy suggests that there are more deep-level radiative recombination centers in sample A, and these energy levels originate from fluctuations in indium components. Based on the micro-PL images, we believe that the indium component fluctuations among the three samples are similar on the plane perpendicular to the epitaxial direction. Therefore, we put forward that an inhomogeneous indium distribution along the epitaxial direction may also contribute to the pronounced difference in the energy level filling effect of the three samples.

Therefore, we want to demonstrate if the inhomogeneous indium distribution along the epitaxial direction is real in our samples. In bulk InGaN materials, component pulling effects have been reported before.[38,39] Due to the lattice mismatch in epitaxial InGaN on GaN materials, the efficiency of indium atom incorporation will be low in the early stages of growth.[40] As the thickness of the InGaN material increases, the lattice mismatch is relatively reduced, leading to higher incorporation of indium atoms into the InGaN lattice. This effect has also been observed in InGaN quantum wells.[34,35] To intuitively demonstrate whether similar effects exist in the three samples in this study, we conducted scanning transmission electron microscopy (STEM) and energy-dispersive x-ray spectroscopy (EDS) analysis on these samples. Traditional characterization methods, such as secondary ion mass spectrometry (SIMS) and cathodoluminescence (CL) energy spectroscopy, are limited by their resolution of about 5–8 nm, which cannot precisely measure the quantum well structure within the thickness range of about 3 nm. Therefore, we chose EDS, despite its semi-quantitative nature. Although the components obtained from EDS testing are not entirely quantitative, the indium content data among these three samples are completely comparable as the EDS tests were conducted almost simultaneously, under the same testing environment. In STEM images, the interfaces in quantum well structures of these three samples are clear. Therefore, we present an image of sample C in Fig. 6(a).

We conducted an analysis of the indium content distribution along the epitaxial growth direction through EDS. The results are depicted in Fig. 6(b). The scanning direction of EDS is indicated in the STEM image (Fig. 6(a)) by a white arrow. Notably, the middle barrier layer, situated between the two wells, exhibits a higher concentration of indium with a more pronounced EDS signal. Conversely, it is hard to detect indium in the lower barrier, adjacent to the n-type layers. The upper barrier layer, near the p-type layers, exhibits indium concentration but is thinner than the designed thickness. The variance in indium concentration between the lower and other two barriers stems from different reaction chamber surroundings during growth, as the indium source during the barrier growth comes partly from residual indium atoms after epitaxy of the former layers. Thus, the lower barrier does not have enough indium source to reach the designed indium content. Furthermore, the reduction in thickness of the upper barrier layer proximate to the p-type layers can be attributed to thermal degradation during the growth of p-type GaN and thermal annealing, a phenomenon that has been previously documented.[41] Thermal annealing can also induce atom diffusion at the surfaces of the barrier and well layers. As illustrated in Fig. 6(b), a gradient in indium content along the epitaxial orientation results from the diffusion of indium atoms between the barrier and well layers.

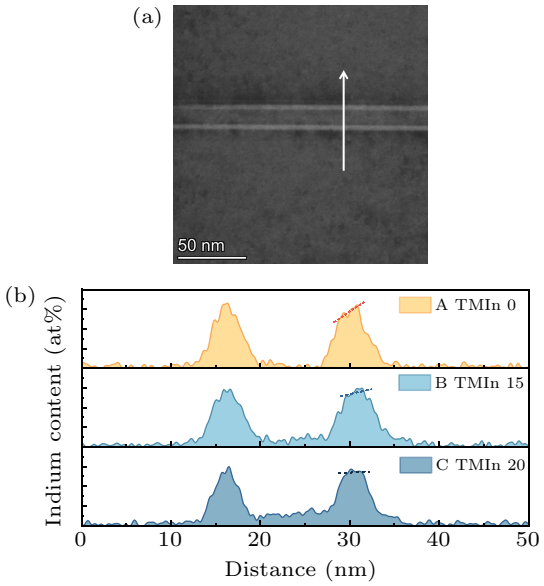


Fig. 6. (a) Cross-section STEM image of sample C, (b) EDS results of samples A, B and C. The white arrow in panel (a) represents the EDS scan direction in panel (b).

The indium distribution within the quantum wells reveals minimal disparity in the overall indium concentration distribution within the first (lower) quantum well along the epitaxial direction, which exhibits sharp triangular shape, with the indium component rapidly escalating and then declining along the growth direction. However, discernible differences emerge in the indium distribution within the second quantum well. Linear fitting was performed on the 3.5 nm-wide region with higher indium concentration within the second quantum well for clearer vision, as depicted in Fig. 9(b). Component distribution in this region delineates the longitudinal distribution

of the indium component within the actual quantum well, as corroborated by HRXRD results in Table 1, as the wells have a thickness of approximately 3.5 nm. Notably, a pronounced component pulling effect is evident in sample A, where increasing quantum well thickness corresponds to a gradual rise in indium composition. Conversely, in samples B and C which have indium in the barrier layers, the component fluctuation is less pronounced, with a relatively uniform component distribution in the 3.5 nm-thick quantum well. Literatures[39,40] suggest that the component pulling effect primarily arises from strain during InGaN growth on GaN. In our samples, a higher indium composition in the barrier layers leads to reduced compressive strain in the subsequent well layers due to the smaller lattice mismatch. Therefore, sample A, with GaN barriers, experiences a substantial lattice mismatch in the second quantum well, leading to pronounced component pulling effects, longitudinal uneven indium distribution and emergence of an In-rich layer. Conversely, samples B and C, with InGaN barrier layers, mitigate lattice mismatch, resulting in less pronounced component pulling effect.

Additionally, the indium component distribution profile in the first quantum well reveals In-rich layers in all three samples. The actual indium content in the first quantum barrier layer is very low, below the detection limit as shown in Fig. 6(b). Consequently, the first quantum barriers in all three samples can be regarded as nearly pure GaN layers, leading to similar stress conditions during the growth of the first quantum well and subsequent exhibition of component pulling effects, culminating in In-rich layers across all samples.

The presence of In-rich layers serves as deep level radiative recombination centers, thereby enhancing carrier filling effects during PL tests in Fig. 4. A simplified schematic diagram illustrating the conduction band structures is presented in Fig. 7 to explain this phenomenon, with arrows denoting the epitaxy direction, considering the polarization effect while disregarding quantization effects. Two samples exhibit different degrees of band tilt. As observed in simulations depicted in Fig. 10, samples featuring InGaN barriers attenuate polarization fields in the well layers, suggesting that the tilt degree of the conduction band in sample A's well layers is larger than those of samples B and C. Furthermore, sample A experiences a more pronounced component pulling effect, resulting in a gradual increase in indium content along the epitaxial direction, thereby augmenting the conduction band tilt. As illustrated in Fig. 7, with a higher degree of conduction band inclination, under identical carrier injection conditions, the energy distribution of carriers in sample A becomes broader, evidenced in TDPL as a larger blue shift in the peak position with increasing temperature. Moreover, considering quantization effects, owing to the substantial tilt of the energy band, the energy trap in sample A is narrower compared to samples B and C under low injection, leading to a greater energy difference between energy levels, particularly for deeper energy levels in the well layers. Consequently, the carrier filling effect induced by the tilt of the energy band is further exacerbated. These effects result in a significantly larger blue shift in the TDPL results of sample A compared to the other two samples.

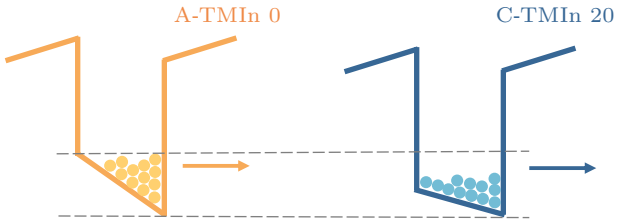


Fig. 7. Simplified schematic diagram of conduction band and carrier filling status of samples A and C under the same small injection, where the build-in electric field is different. The arrows represent the epitaxy direction.

Based on the experimental analysis of the influence of barrier indium content on MQW quality, higher indium content in barrier layers partly diminishes the indium incorporation efficiency in well layers but can mitigate the component pulling effect by reducing the lattice mismatch. Higher indium content in barrier layers effectively enhances the indium content homogeneity along the epitaxial direction. Apart from this, in light of the disparity in homogeneity and indium incorporation efficiency, samples featuring higher indium content in barrier layers exhibit a broader effective band gap, resulting in a blue shift in emission wavelength. When it comes to LD structure, the enhanced homogeneity of MQW with higher indium content barriers lowers the threshold current of LDs. These findings support the diverse performance properties of LDs outlined in Fig. 2.

3.3. Computational results of LDs with different barrier layers

Apart from material quality of MQW, different indium contents in barrier layers may also influence LD's performance by modulating optical confinement ability and carrier recombination efficiency. Thus, we employed simulation methods via LASTIP to investigate the influence of structural differences from device physics aspect as a supplement to the experimental analysis part. Five distinct samples were established with varying barrier indium compositions: 0%, 1%, 2%, 3%, and 4%. Firstly, the *P*–*I* curves of these samples are depicted in Fig. 8(a), with threshold currents and slope efficiencies shown in Fig. 8(b). Despite the sample with 4% indium content in the barrier, increasing indium content in the barrier effectively enhances LD performance, as evidenced by the increase in slope efficiency and decrease in threshold current. The sample with a 4% indium content barrier exhibits relatively poor performance. Notably, the indium contents of the lower and upper waveguide (LWG and UWG) layers of LDs are both set to 4% according to the real LD structure. We

propose that the performance difference can be attributed to variations in optical field distribution.

The optical confinement factors of the samples are illustrated in Fig. 8(c). Due to the refractive index difference between the quantum barrier and waveguide layers in samples with barrier indium contents ranging from 0% to 3%, higher indium content in the barriers results in a higher effective refractive index,[23] thereby increasing the optical confinement factor and improving the LD output performance. However, when the indium content of the barrier matches that of the waveguide layers, the optical confinement factor decreases, leading to a deterioration in LD performance.

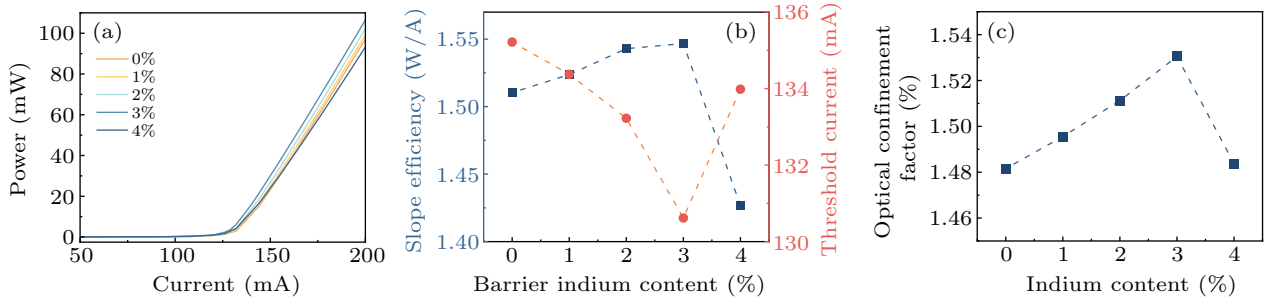


Fig. 8. Simulation results of (a) *P–I* curves, (b) slope efficiency, threshold current and (c) optical confinement factor change with different barrier indium contents.

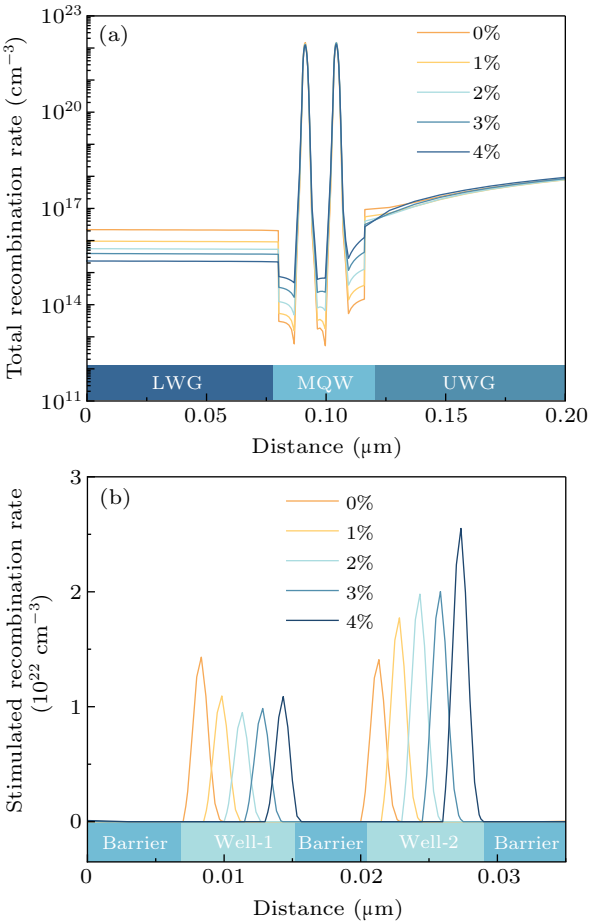


Fig. 9. Total carrier recombination rate (a) and stimulated recombination rate (b) distribution along the epitaxy direction at 200 mA. The position of each quantum well in (b) is manually shifted by 1.5 nm in turn for clear eye view. The exact quantum well position during simulation is kept the same.

On the other hand, we extracted the total recombination rates and stimulated recombination rates when lasing at 200 mA, as depicted in Fig. 9. In Fig. 9(a), the total recombination rate in LWG experiences a significant decrease when the indium content in barriers is increased. Specifically, the total recombination rate in the LWG of the GaN barrier sample is 2.1×10^{16} cm^{-3}, whereas that of the $In_{0.04}Ga_{0.96}N$ barrier sample is 2.2×10^{15} cm^{-3}. This magnitude difference indicates that carrier recombination loss out of the active region is effectively reduced with a high indium content barrier structure. Furthermore, the total stimulated recombination rate, as illustrated in Fig. 9(b), reinforces this point. Samples with higher indium content barriers exhibit a higher total stimulated recombination rate from the two well layers, directly reflecting the improvement in LD performance.

For a clearer understanding of these performance differences, the band structures of samples with GaN barrier and $In_{0.04}Ga_{0.96}N$ barrier at 0 V, along with corresponding carrier wave functions in the quantum wells, are presented in Figs. 10(a) and 10(b), respectively. Due to the indium component disparity between waveguide layers and barriers, injection barrier potentials exist during both hole and electron injections. As depicted in marks 1 and 2 in Fig. 10, the hole injection barrier potential is reduced by the higher indium content barrier layer. Similarly, as shown in marks 3 and 4 in Fig. 10, the electron injection potential is significantly reduced as well. Consequently, lower electron concentrations can be observed in LWG in samples with higher indium content barriers, leading to reduced carrier recombination out of the active region in the LWG, as discussed in Fig. 9. Similar effects have been reported elsewhere in GaN based green laser diodes,[42] and this explains why LD performance is enhanced with higher indium content barriers.

Additionally, increasing the indium content in the barrier layer does not always guarantee improved performance, as demonstrated by the LD with $In_{0.04}Ga_{0.96}N$ barriers exhibiting a performance decrease. Taking into account the component difference between barrier and well layers, for a specific target lasing wavelength, higher indium content in barriers will re-

duce the effective well depth. Referring to the quantum wave function of carriers shown in Fig. 10, where the baseline of wave functions represents the energy level of carriers in the well layers, it is evident that with an increase in barrier indium content, the number of possible energy levels in the quantum well decreases. In our simulation, the indium content of barrier layers is not excessively high. However, with higher indium content, the wave function in the quantum well region extends beyond the quantum well region. This will reduce the overlap between hole and electron wave functions, reducing the carrier recombination efficiency. Furthermore, we label the energy gap between the ground levels of holes and electrons in Fig. 10 to represent the lasing wavelength. The energy gap of the sample with GaN barrier is 2.821 eV, which is higher than the 2.805 eV of the sample with $In_{0.04}Ga_{0.96}N$ barrier. In this case, high indium composition in the barrier layers partly shields the polarization electric field in the well layers, decreasing the tilt of the band structure, and shortening the ground state level gap between electrons and holes, resulting in a red-shift in the lasing wavelength. The lasing wavelength of the sample with GaN barrier is 440.1 nm, while the lasing wavelength of the sample with $In_{0.04}Ga_{0.96}N$ barrier is 441.9 nm from simulation results. Although this result does not align well with experimental results in LD or MQW samples owing to realistic indium incorporation related issues, such differences in simulation should also be taken into consideration when designing the target wavelength during real LD fabrication.

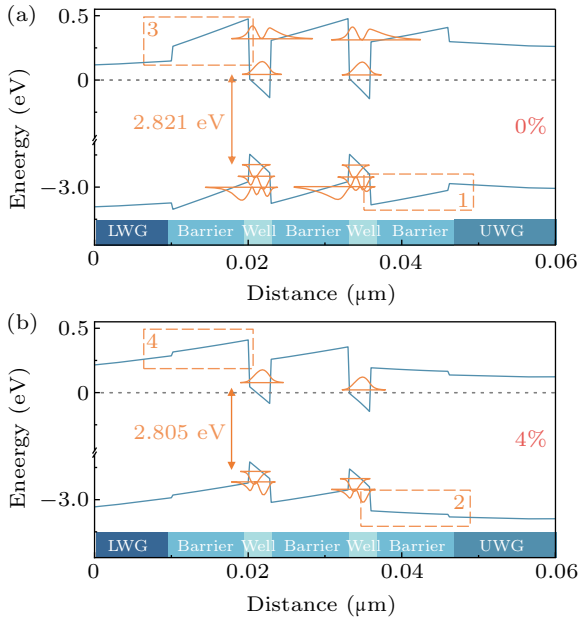


Fig. 10. Band structure diagrams and ground and excited states wave functions of carriers in quantum wells at 0 V for two samples with (a) 0% and (b) 4% barrier indium content.

4. Conclusion

In the pursuit of high efficiency and high output power GaN-based blue laser diodes (LDs), the choice of barrier layers emerges as a crucial consideration. Our fabrication of LD samples with InGaN barrier layers revealed that higher indium content in these layers is correlated with lower threshold current densities and shorter lasing wavelengths. Through both theoretical calculation and experimental study, InGaN barrier layers demonstrate clear advantages over GaN barrier layers in both device physics analysis and actual material growth. It is found that higher indium content in barrier layers can partly suppress indium composition in well layers. More importantly, higher indium content barriers effectively enhance carrier recombination efficiency and indium content homogeneity in quantum well layers, thereby improving the output performance of GaN-based blue LDs.

Acknowledgments

Project supported by Youth Innovation Promotion Association of the Chinese Academy of Sciences (Grant No. 2023124), the National Key Research and Development Program of China (Grant No. 2022YFB3608100), Key Research and Development Program of Jiangsu Province (Grant No. BE2021008-1), Shanxi-Zheda Institute of Advanced Materials and Chemical Engineering (Grant No. 2022SX-TD016), the National Natural Science Foundation of China (Grant Nos. 62274157, 61904172, 62127807, 62234011, 61974162, 62034008, 62074142, 62074140, and 62250038), and Strategic Priority Research Program of Chinese Academy of Sciences (Grant No. XDB43030101).

References

[1] Nakatsu Y, Nagao Y, Hirao T, Hara Y, Masui S, Yanamoto T, Nagahama S I, Morkoç H, Fujioka H and Schwarz U T 2020 *Gallium Nitride Materials and Devices XV* 2020
[2] Yang J, Zhao D, Liu Z, Liang F, Chen P, Duan L, Wang H and Shi Y 2022 *J. Semiconduct.* **43** 010501
[3] Liang F, Zhao D, Liu Z, Chen P, Yang J, Duan L, Shi Y and Wang H 2021 *J. Semiconduct.* **42** 112801
[4] Li Z, Liu J, Feng M, Zhou K, Zhang S, Wang H, Li D, Zhang L, Zhao D, Jiang D, Wang H and Yang H 2013 *Appl. Phys. Lett.* **103** 152109
[5] Zhi T, Tao T, Liu X, Xue J, Wang J, Tao Z, Li Y, Xie Z and Liu B 2021 *J. Semiconduct.* **42** 122803
[6] Chyi J I, Nanishi Y, Morkoç H, Piprek J, Yoon E, Fujioka H, Strauß U, Hager T, Brüderl G, Wurm T, Somers A, Eichler C, Vierheilig C, Löffler A, Ristic J and Avramescu A 2014 *Gallium Nitride Materials and Devices IX* 2014
[7] Murayama M, Nakayama Y, Yamazaki K, Hoshina Y, Watanabe H, Futagawa N, Kawanishi H, Uemura T and Narui H 2017 *Phys. Status Solidi (a)* **215** 1700513
[8] Cheng L, Zhang J, Wang J, Zhang J, Yang J, Wu S, Qian Q and Chen H 2021 *J. Appl. Phys.* **130** 183104
[9] Alam S, Sundaram S, Li X, Jamroz M E, El Gmili Y, Robin I C, Voss P L, Salvestrini J P and Ougazzaden A 2017 *Phys. Status Solidi (a)* **214** 1600868
[10] Park S H 2015 *J. Korean Phys. Soc.* **66** 277
[11] Park S H, Moon Y T, Lee J S, Kwon H K, Park J S and Ahn D 2010 *Appl. Phys. Lett.* **97** 121107
[12] Park S H, Chung T H, Baek J H and Ahn D 2015 *Jpn. J. Appl. Phys.* **54** 022101
[13] Fu H, Sun W, Ogidi-Ekoko O, Goodrich J C and Tansu N 2019 *AIP Adv.* **9** 045013
[14] Kuo Y K, Chang J Y, Tsai M C and Yen S H 2009 *Appl. Phys. Lett.* **95** 011116

[15] Wang T C, Ko T S, Lu T C, Kuo H C, Gao R C, Tsay J D and Wang S C 2008 *Phys. Status Solidi c* **5** 2161
[16] Streubel K P, Wang T H, Jeon H, Chang J Y, Tsai M C, Tu L W, Linder N and Kuo Y K 2011 *Light-Emitting Diodes: Materials, Devices, and Applications for Solid State Lighting XV* 2011
[17] Yang Y and Zeng Y 2015 *J. Appl. Phys.* **117** 035705
[18] Noh Y K, Kim M D and Oh J E 2011 *J. Appl. Phys.* **110**
[19] Chung H Y, Woo K Y, Kim S J and Kim T G 2014 *Opt. Commun.* **331** 282
[20] Wang W J, Liao M L, Yuan J, Luo S Y and Huang F 2022 *Chin. Phys. B* **31** 074206
[21] Ben Y, Liang F, Zhao D, Yang J, Liu Z and Chen P 2022 *Opt. Laser Technol.* **145** 107523
[22] Mahala P, Behura S K, Ray A, Dhanavantri C and Jani O 2015 *Opt. Quant. Electron.* **47** 1117
[23] Laws G, Larkins E, Harrison I, Molloy C and Somerford D 2001 *J. Appl. Phys.* **89** 1108
[24] Lu D and Duan S 2000 *Chin. J. Semiconduct.* **21** 105
[25] Ambacher O, Smart J, Shealy J R, Weimann N G, Chu K, Murphy M, Schaff W J, Eastman L F, Dimitrov R, Wittmer L, Stutzmann M, Rieger W and Hilsenbeck J 1999 *J. Appl. Phys.* **85** 3222
[26] Takeuchi T, Wetzel C, Yamaguchi S, Sakai H, Amano H, Akasaki I, Kaneko Y, Nakagawa S, Yamaoka Y and Yamada N 1998 *Appl. Phys. Lett.* **73** 1691
[27] Vurgaftman I, Meyer J R and Ram Mohan L R 2001 *J. Appl. Phys.* **89** 5815
[28] Mccluskey M, Van De Walle C, Master C, Romano L and Johnson N 1998 *Appl. Phys. Lett.* **72** 2725
[29] Cho Y H, Gainer G H, Fischer A J, Song J J, Keller S, Mishra U K and Denbaars S P 1998 *Appl. Phys. Lett.* **73** 1370
[30] Manoogian A and Woolley J C 1984 *Can. J. Phys.* **62** 285
[31] Danhof J, Vierheilig C, Schwarz U T, Meyer T, Peter M and Hahn B 2011 *Phys. Status Solidi (b)* **248** 1270
[32] Wang X and Xu S 2022 *Chin. Phys. Lett.* **39** 107801
[33] Langer T, Pietscher H G, Ketzer F A, Jönen H, Bremers H, Rossow U, Menzel D and Hangleiter A 2014 *Phys. Rev. B* **90** 205302
[34] Hao M, Ishikawa H, Egawa T, Shao C L and Jimbo T 2003 *Appl. Phys. Lett.* **82** 4702
[35] Ben Y, Liang F, Zhao D, Yang J, Chen P and Liu Z 2022 *J. Mater. Res. Technol.* **21** 2228
[36] Eliseev P G, Perlin P, Lee J Y and Osinski M 1997 *Appl. Phys. Lett.* **71** 569
[37] Bai J, Wang T and Sakai S 2000 *J. Appl. Phys.* **88** 4729
[38] Hiramatsu K, Kawaguchi Y, Shimizu M, Sawaki N, Zheleva T, Davis R F, Tsuda H, Taki W, Kuwano N and Oki K 1997 *Mrs Internet Journal of Nitride Semiconductor Research* **2** U3
[39] Pereira S, Correia M R, Pereira E, O'donnell K P, Trager-Cowan C, Sweeney F and Alves E 2001 *Phys. Rev. B* **64** 205311
[40] Inatomi Y, Kangawa Y, Ito T, Suski T, Kumagai Y, Kakimoto K and Koukitu A 2017 *Jpn. J. Appl. Phys.* **56** 078003
[41] Chen Z, Liang F, Zhao D, Yang J and Liu Z 2024 *J. Alloys Compd.* **983** 173909
[42] Chen Z, Liang F, Zhao D, Yang J, Chen P and Jiang D 2022 *Nanomaterials* **12** 2581